

Pairwise Nonlinear Dependence Analysis of Genomic Data

Siqi Xiang¹, Siyao Liu^{2,3,4}, Charles M. Perou², Kai Zhang¹, and J. S. Marron^{1,2}

¹*Department of Statistics and Operations Research, University of North Carolina at Chapel Hill*

²*Lineberger Comprehensive Cancer Center, University of North Carolina at Chapel Hill*

³*Department of Genetics, School of Medicine, University of North Carolina at Chapel Hill*

⁴*Curriculum in Bioinformatics and Computational Biology, University of North Carolina at Chapel Hill*

xsiqui@email.unc.edu, siyao@email.unc.edu, cperou@med.unc.edu, zhangk@email.unc.edu, marron@unc.edu

Abstract

In The Cancer Genome Atlas (TCGA) dataset, there are many interesting nonlinear dependencies between pairs of genes that reveal important relationships and subtypes of cancer. Such genomic data analysis requires a rapid, powerful and interpretable detection process, especially in a high-dimensional environment. We study the nonlinear patterns among the expression of genes from TCGA using a powerful tool called Binary Expansion Testing. We find many nonlinear patterns, some of which are driven by known cancer subtypes, some of which are novel.

Keywords— Binary Expansion, Genomic data, Nonlinear dependence, Nonparametric dependence testing

1 Introduction

A leading cause of death in the world is cancer. A lot of cancer research is currently analyzing larger and larger data sets. In this paper, we focus on The Cancer Genome Atlas (TCGA) (2012), which is a particularly important and comprehensive data set to study cancer biology and genomics. It is a publicly available genomics data resource that seeks to understand several types of cancer by collecting multiple diverse data over many people. In that set, an important data type is gene expression, and more specifically, RNA-seq data. A biologically useful task of modern genomics data analysis is detecting the dependency patterns among gene expression. Conventional approaches to dependency, such as Pearson's, Spearman's rank, or Kendall's rank correlation coefficients, target linear dependence. Here we investigate nonlinear dependence in TCGA breast cancer data set. An example of the expression of two genes with strong and important nonlinear dependence that is not discoverable by linear methods is shown in the left panel of Figure 1. That is a scatter plot of expression for the genes BCL11A and F2RL2. For this pair of genes, the Pearson correlation coefficient is -0.0069, Spearman's ρ is 0.088, and Kendall's τ is 0.085. These correlation coefficients are close to zero, suggesting no linear correlation between these two genes, as is also visually

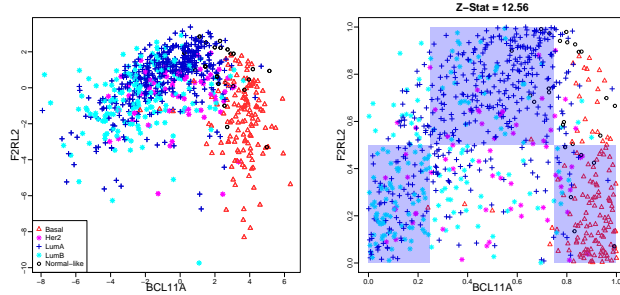


Figure 1: Left: The scatter plot comparing expression of two genes in TCGA breast cancer data in the normalized log count scale; Right: The scatter plot of the same two genes using a copula transformation with the nonlinearity pattern from BET. The z-statistic of BET is 12.84. These pairwise genes exhibit an interesting nonlinear dependence pattern which is explained by showing the breast cancer subtypes.

apparent. However, there is clear nonlinear dependence. This dependence is explained from a biological viewpoint by labeling with commonly used breast cancer subtypes [Parker et al., 2009]. As shown by the colors and symbols in Figure 1, the decreasing part on the right is mainly composed of the Basal (\triangle) subtype observations. The increasing part on the left is driven by the Luminal A (+) and Luminal B (*) subtypes. This nonlinear dependence pattern has been discovered by Binary Expansion Testing (BET) proposed by Zhang [2019]. The right panel of Figure 1 is the corresponding BET diagnostic plot explained in Section 2.1.

The data set studied in this paper consists of gene expression features of TCGA Lobular Freeze breast cancer data from Ciriello et al. [2015], containing 16615 genes. Note that the total number of pairwise comparisons of genes is $\binom{16615}{2} = 138,020,805$. Human visualization of all of these scatter plots is intractable [Sun and Zhao, 2014]. An interesting early approach to this is Tukey’s scagnostics [Wilkinson et al., 2005]. The large number of pairs motivates a computationally efficient method for investigating pairwise dependence. Gene expression studies have revealed a large number of linear dependencies between genes. In particular, in our BET analysis, we discover 10,110,787 pairs of (statistically significant using Bonferroni multiple comparison adjustment) dependencies between genes. A large number of these are well understood. This paper takes genomics in a new direction by investigating nonlinear dependencies of the type shown in Figure 1.

There are several current approaches to studying nonlinear dependence. An early measure was Hoeffding’s D [Hoeffding, 1948] which is not particularly powerful. More recently, Székely et al. have proposed the more powerful method of distance correlation [Székely et al., 2007, Székely and Rizzo, 2013]. Another more powerful approach is the k -nearest neighbor mutual information (KNN-MI) algorithm [Kraskov et al., 2004, Kinney and Atwal, 2014], which focuses on mixtures of gaussian distributions. While these methods are beneficial for discovering nonlinear dependence, they are less suitable for extensive genomic studies for three reasons. First, they are not efficient for large-scale computation problems such as TCGA data (10s of thousands of genes and samples). Second, they still face some power loss, as noted using simulation studies in Section 6 of Zhang [2019]. Third, there is less immediate interpretation of the type that is available from BET.

To demonstrate the relatively slow execution time needed for the three methods above, we compare the calculation speed of BET with these three methods. The running time for testing all

pairs of a randomly selected set of 100 genes is shown in Table 1. We use the default setting for each algorithm.

Table 1: The running time of the pairwise comparison of 100 genes. The more powerful nonlinear detection methods are orders of magnitude slower than BET.

| Algorithms | BET | Hoeffding's D | Distance Correlation | KNN Mutual Information |
|------------|-----------|---------------|----------------------|------------------------|
| Times | 8.96 secs | 24.05 secs | 17.51 mins | 4.91 hours |

Table 1 shows that BET is around three times faster than the much less powerful Hoeffding's D. It also shows that BET provides computational speed that is several orders of magnitude faster than either distance correlation or KNN mutual information in the context of dependence testing of high-dimensional data such as TCGA. Nonlinear dependence can arise in many forms. Another advantage of BET is that it gives additional information on the form of nonlinear dependence, as illustrated in Figure 2.

This paper is organized as follows. Section 2 describes the main idea of the Binary Expansion Testing (BET) algorithm. Section 3 details the BET analysis of the TCGA data set, revealing several interesting nonlinear patterns. Section 4 studies the validation of some surprising TCGA results using an independent genomics data set. Section 5 concludes the article.

2 Binary Expansion Testing for Nonlinear Dependency Detection

BET is a recent and innovative approach for dependence testing that is powerful for detecting pairwise nonlinear dependence. Furthermore, it provides a computationally fast investigation process for large-scale data sets, as shown in Table 1. Finally, BET gives a clear interpretation for some specific nonlinear dependence patterns. These patterns are formally introduced in Section 2.1. The BET algorithm and inference are given in Section 2.2.

2.1 BET Dependence Patterns

The input to BET is the copula transform of the bivariate distribution, i.e., a marginal probability integral transformation of each variable in the pair. The key idea of BET is to partition the unit square $[0, 1]^2$ into different patterns that can approximate the dependence between two marginal uniform random variables U and V . For fast computation, these patterns are dyadic in nature. The first few of these are shown in Figure 2 as blue and white blocks. Each partition pattern is called a *Binary Interaction Design (BID)* by Zhang [2019]. The BIDs are parametrized by the specific depths d_1 and d_2 . We choose the depths $d_1 = 2$ and $d_2 = 2$ in our genomics data analysis which results in nine dependence BIDs shown in Figure 2. Each BID corresponds to one BET dependence type. If there is no dependence between U and V , the observations are distributed in $[0, 1]^2$ randomly. Hence we expect a similar count of points in the white and the blue regions, i.e., the unions of the white (and blue respectively) rectangles. When there are some dependencies, we expect a significant difference between these counts of points S (called the *symmetry statistic*), for some forms of BIDs. The value of S is given for each BID in Figure 2. Notice that S is positive

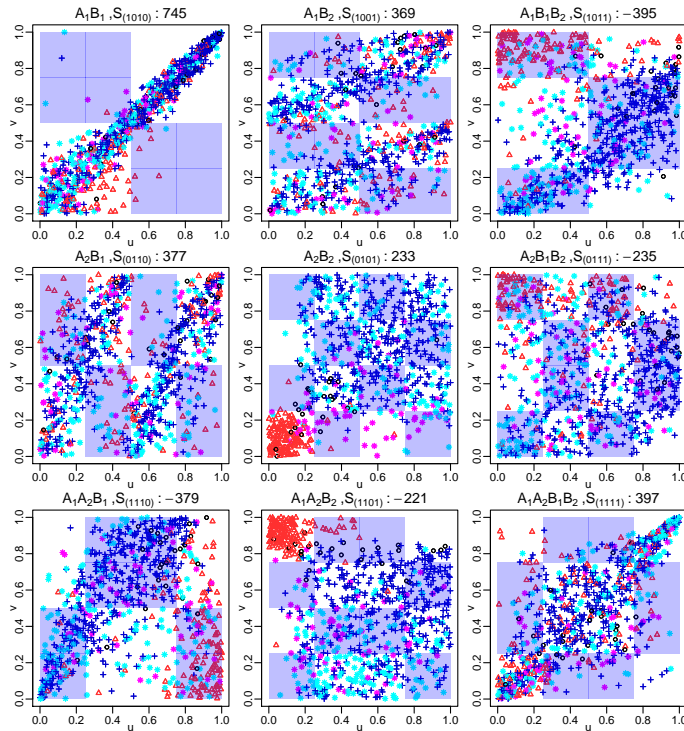


Figure 2: The first nine dyadic binary interaction designs (BIDs) used by BET with the given depths $d_1 = d_2 = 2$ and one example pair of expression data shown for every BID, with S indicating the difference of counts in white and blue regions. Each BID is aimed at detecting a particular dependence relationship between two $[0, 1]$ uniform random variables. Size of S indicates the strength of nonlinear dependence in each BID. A number of biologically relevant patterns are shown.

if the white part is denser than the blue and negative otherwise. For example, the white region in the upper-left panel of Figure 2 (the label A_1B_1 of that BID will be explained later) contains more points and captures a monotone upward dependence, which corresponds to a large positive S . If it is downward linear, there will be greater density in the blue region, and S will be statistically significantly negative. Each dependence pattern in Figure 2 is illustrated using a pair of genes that strongly exhibits the corresponding BID, particularly the pair with the maximal absolute value of S .

From Figure 2, BET captures several different nonlinear relationships for strongly dependent pairs of genes. Specific genes in these pairs are listed in Table 2, where Gene 1 (U) is on the horizontal axis and Gene 2 (V) is on the vertical axis. As noted above, the symmetry statistic S for each BID is far from 0, indicating that solid dependency exists. For example, the middle-left highlights a surprising bimodal pattern that we will discuss in detail in Section 3.5 and 4.1. The bottom-left indicates dependence roughly following a downward opening parabola, which is captured by the blue region and has a negative S value because the blue region contains many more points. Dependence like an upward opening parabola would have a large positive value of S because of a higher density of points in the white region. Left and right opening parabolas are captured by the BID in the upper-right, where this pair of genes has a leftward opening parabola. In contrast, the bottom-right panel looks quite different. It is fairly close to linear dependence, but clearly not bivariate normal. There are unusual concentrations in the upper right and the lower left.

The prevalence of these mixture patterns and some of the others frequently turns out to be a

Table 2: Gene names for each pair in Figure 2

| Location | Gene 1 (U) | Gene 2 (V) |
|---------------|----------------|----------------|
| top-left | C17orf81 | C17orf61 |
| top-middle | RPL24 | RPL9 |
| top-right | JAM3 | ANKS6 |
| middle-left | RPL9 | RPL32 |
| center | PRR15 | CA12 |
| middle-right | CDH5 | ZNF883 |
| bottom-left | ANKS6 | DCN |
| bottom-middle | CT62 | FAM174A |
| bottom-right | PROSC | ASH2L |

consequence of known breast cancer subtypes. In particular, Basal is known to be very distinct. The dependencies highlighted by a number of different BIDs in Figure 2 are clearly explained by the separation between Basal (\triangle) and the other subtypes. The two mixture patterns, in the bottom-left and the top-right BIDs, demonstrate how the mixture of Basal and other subtypes can drive such patterns. The great difference between the Basal subtype and the rest also drives the dependency patterns in the center (A_2B_2) and the bottom-middle ($A_1A_2B_2$) BIDs. It is important to remember that several BIDs can respond (have a significant absolute value of S) to a given dependence pattern in the data, but we show just the one with the largest absolute value for each pair of genes of S . This data set has a perhaps surprising amount of dependence, as seen from the numbers of significant gene pairs shown in Figure 4.

2.2 BET Algorithm and Inference

Next we formally introduce the testing procedure and notations. For each pair of genes, consider the sample data as pairs of variables $(X_1, Y_1), \dots, (X_n, Y_n)$. We view these as realizations of two random variables X and Y . BET is a fully nonparametric method based on the copula transformation, which is computed from the marginal CDFs. In particular, let $U = F_X(X)$ and $V = F_Y(Y)$ which are uniform on $[0, 1]$ and preserve the relative relationship between X and Y . Because the CDFs $F_X(X)$ and $F_Y(Y)$ are often unknown in practice, BET approximates them using the empirical CDF. Thus the i th observation in the empirical copula is (\hat{U}_i, \hat{V}_i) whose marginal distribution is uniformly distributed on the equally spaced support points $\frac{1}{n}, \dots, \frac{n-1}{n}, 1$ on $[0, 1]$.

A key motivation for BET is that each decimal fraction number in the interval $[0, 1]$ has a binary representation. Because of the binary patterns that underlie Figure 2, the probabilistic binary expansions of the continuous random variables U and V are particularly useful. These binary expansions [Kac, 1959] are $U = \sum_{k=1}^{\infty} A_k/2^k$ and $V = \sum_{k'=1}^{\infty} B_{k'}/2^{k'}$, where $A_k \stackrel{iid}{\sim} \text{Bernoulli}(1/2)$ and $B_{k'} \stackrel{iid}{\sim} \text{Bernoulli}(1/2)$. Similarly, each observation in the empirical copula \hat{U}_i and \hat{V}_i also has a binary expansion: $\hat{U}_i = \sum_{k=1}^{\infty} \hat{A}_{k,i}/2^k$ and $\hat{V}_i = \sum_{k'=1}^{\infty} \hat{B}_{k',i}/2^{k'}$. Note that the binary expansion of an observation \hat{U}_i is the binary representation of this number. Thus, \hat{A}_k and $\hat{B}_{k'}$ can be regarded as the 0-1 indicator functions containing the randomness of \hat{U}_i and \hat{V}_i , for example, $\hat{A}_1 = I(\hat{U}_i \in (1/2, 1])$ and $\hat{A}_k = I(\hat{U}_i \in \cup_{k=1}^{k-1} (2k - 1/2^{k-1}, 2k/2^k])$. The BET framework is

based on the truncation of these binary expansions at some finite depths d_1 and d_2 , respectively, $U_{d_1} = \sum_{k=1}^{d_1} A_k/2^k$ and $V_{d_2} = \sum_{k'=1}^{d_2} B_{k'}/2^{k'}$. The discrete variables U_{d_1} and V_{d_2} take on at most 2^{d_1} and 2^{d_2} values. Thus, there are $2^{d_1+d_2-1}$ binary variables resulting from interactions between A_k and $B_{k'}$. These variables are sufficient statistics to study dependence [Zhang, 2019]. In order to present these interaction variables in the form of products and reflect dependence between these products, we use the binary variables $\dot{A}_k = 2A_k - 1$ and $\dot{B}_{k'} = 2B_{k'} - 1$ to replace A_k and $B_{k'}$. Thus the interaction events between A_k and $B_{k'}$ can be written as the products $\dot{A}_k \dot{B}_{k'}$. For example, the events $\{A_1 = 1, B_1 = 1\}$ and $\{A_1 = 0, B_1 = 0\}$ lead to the same interaction event $\{\dot{A}_1 \dot{B}_1 = 1\}$. Out of these $2^{d_1+d_2-1}$ interactions, there are $(2^{d_1} - 1)(2^{d_2} - 1)$ variables of form $\dot{A}_{k_1} \dots \dot{A}_{k_r} \dot{B}_{k'_1} \dots \dot{B}_{k'_t}$ for some $r, t > 0$. We call these variables *cross interactions*, each of which results from the product of at least one \dot{A}_k and one $\dot{B}_{k'}$ and reflects a BET partition (the BID mentioned earlier) in $[0, 1]^2$. Figure 2 shows the BIDs for all nine cross interaction variables with the given depths $d_1 = d_2 = 2$. Let \mathbf{a} and \mathbf{b} denote vectors of length d_1 and d_2 with 1's at $k_1 \dots k_r$ and $k'_1 \dots k'_t$ respectively and 0's otherwise, thus we can denote the cross interaction $\dot{A}_{k_1} \dots \dot{A}_{k_r} \dot{B}_{k'_1} \dots \dot{B}_{k'_t}$ as $\dot{A}_{\mathbf{a}} \dot{B}_{\mathbf{b}}$. For simplicity of notation, the labels $A_{\mathbf{a}} B_{\mathbf{b}}$ in most figures represent the cross interactions $\dot{A}_{\mathbf{a}} \dot{B}_{\mathbf{b}}$. For example, in Figure 2, the BID $A_1 B_1$ represents the cross interaction variable $\dot{A}_1 \dot{B}_1$, where the observation i in the white region reflects the event $\{\dot{A}_{1,i} \dot{B}_{1,i} = 1\}$ and in the blue region reflects the event $\{\dot{A}_{1,i} \dot{B}_{1,i} = -1\}$.

Now we can calculate the symmetry statistic S , the difference of counts in white and blue regions for a cross interaction $\dot{A}_{\mathbf{a}} \dot{B}_{\mathbf{b}}$, as the sum of the observed binary interaction variables $S_{(\mathbf{a}\mathbf{b})} = \sum_{i=1}^n \dot{A}_{\mathbf{a},i} \dot{B}_{\mathbf{b},i}$, where $\mathbf{a}\mathbf{b}$ is the concatenation of \mathbf{a} and \mathbf{b} . The U_{d_1} and V_{d_2} are strongly dependent when the absolute value $|S_{(\mathbf{a}\mathbf{b})}|$ is far from zero for at least one BID, according to the following fundamental observation of Zhang [2019]: If U_{d_1} and V_{d_2} are independent, the symmetry statistic $S_{(\mathbf{a}\mathbf{b})}$ satisfies $(S_{(\mathbf{a}\mathbf{b})} + n)/2 \sim \text{Binomial}(n, 1/2)$, for $\mathbf{a} \neq 0$ and $\mathbf{b} \neq 0$. If the empirical copula transformation is used, we can use $\hat{S}_{(\mathbf{a}\mathbf{b})} = \sum_{i=1}^n \hat{\dot{A}}_{\mathbf{a},i} \hat{\dot{B}}_{\mathbf{b},i}$ as the symmetry statistic and $(\hat{S}_{(\mathbf{a}\mathbf{b})} + n)/4 \sim \text{Hypergeometric}(n, n/2, n/2)$, for $\mathbf{a} \neq 0$ and $\mathbf{b} \neq 0$.

The Max BET procedure of Zhang [2019] at depths d_1 and d_2 is described as follows for a given pair of variables. First, we compute all symmetry statistics with cross interactions for the given d_1 and d_2 . Then we look for the symmetry statistic with the strongest asymmetry and record its p-value and z-statistic $|S_{(\mathbf{a}\mathbf{b})}|/\sqrt{n}$. Finally, we use a Bonferroni adjustment to obtain the family-wise error rate p-value. For each pair of testing variables, the dependence relationship is represented by the most significant BID.

Notice that there is a reflection property among the BIDs. For example, the BIDs $A_1 B_1 B_2$ and $A_1 A_2 B_1$ represent the same relationship up to a switch of the axis positions (i.e., reversal of the roles of the two genes) for the two random variables U and V . There are three pairs of such reflected patterns. Identifying such pairs results in six BID patterns: five nonlinear and one linearity. It will be seen in Section 3.3 that both parts of reflected patterns should be considered.

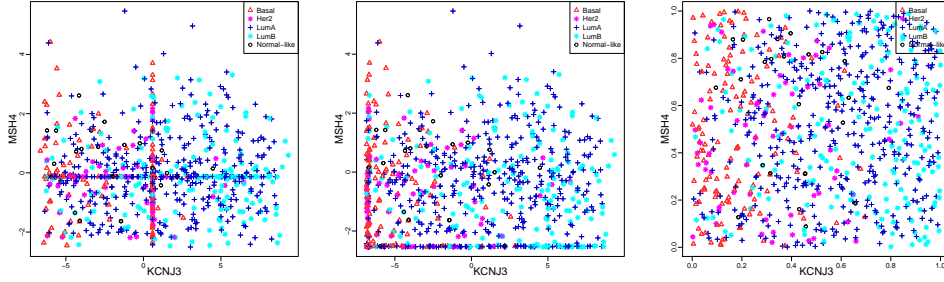


Figure 3: Left: The scatter plot comparing expression of two genes in the TCGA breast cancer data in the normalized log count scale with zero value imputation by the median; Middle: The scatter plot of the same two genes in the normalized log count scale with resetting the median to the minimum and jittering to nonunique values; Right: The scatter plot of the same two genes in the copula distribution scale.

3 Results From TCGA

In this section, we first expand on the data preprocessing of TCGA data set in Section 3.1. Then we summarize the analysis results in Section 3.2. Finally, we discuss some specific nonlinear dependency patterns in the last few subsections.

3.1 Data Preprocessing

The RNA-seq gene expression features of TCGA Lobular Freeze breast cancer data set from Ciriello et al. [2015] contain 16615 genes of 817 primary tumor samples, including five subtypes: Basal-like, HER2, Luminal A, Luminal B, and Normal-like. Intrinsic breast cancer subtyping was done using the PAM50 classifier [Parker et al., 2009].

Gene expression data is naturally analyzed on the log scale. During genomics data preprocessing, each sample was normalized to a fixed upper quartile and then log2 transformed. Genes with zero values following the log2 transformation were set as missing and genes with missing values in more than 20% of the samples were excluded. In the following imputation process, these zeros (marked as missing values after log transformation) were replaced by the median for that gene after the log transformation. The left panel in Figure 3 shows an example pair of genes with many points piled up at the median representing missing values because zeros are not defined on the log scale. There are some drawbacks to handling the zeros in that way because all these data are based on counts, so zero should be the smallest. Thus, in our preprocessing step, all but the first of the median values are set to a minimum value because we have an odd number of 817 samples. Hence the first median observation is left at the sample median. The result of this process is shown in the middle panel of Figure 3. This causes many ties for the smallest value, and a large number of ties will strongly impact the BET inference. Therefore these points are spread out using a jitter approach. To preserve the ranks, a small random value (uniformly distributed between the minimum and second minimum) is added to the non-unique minimum observations. Finally, we apply the empirical copula transformation. See the right panel in Figure 3.

As noted in Parker et al. [2009], these subtypes play a critical role in many aspects of breast cancer. Our analysis in Section 3.3 confirms that the Basal subtype tends to be quite different

from the rest. Hence, We also investigate the context of LumA/LumB/Her2, which tends to be dominated by the most numerous subtype LumA. We further investigate the non-LumA group, meaning the union of Her2/LumB, and LumA separately. Hence our analysis focuses on the four different contexts shown in Table 3 which are chosen to highlight important aspects. Note that the BET analysis focuses on detecting nonlinearity but not subtypes. However, there is a relationship between nonlinearity and subtypes. We set the depth parameters in the BET algorithm d_1, d_2 to be 2, and only focus on five nonlinear BIDs, as discussed in Section 2.2. To control multiple comparisons, we modify the p-value using Bonferroni’s corrected p-value and then use the level 0.05.

Table 3: Four contexts and the corresponding sample sizes.

| Contexts | All five subtypes | LumA/LumB/Her2 | Her2/LumB | LumA |
|--------------|-------------------|----------------|-----------|------|
| Sample Sizes | 817 | 656 | 241 | 415 |

The BET detection results of TCGA breast cancer data for these four different contexts and five nonlinear BIDs are summarized in Section 3.2. More detailed descriptions are in Section 3.3 through Section 3.6.

3.2 Summary of BET Analysis

As we discussed at the end of Section 2.2, there are three pairs of reflected nonlinear BIDs in all nine BIDs. Identifying such pairs results in five nonlinear BIDs, see the five columns of Figure 4. From this point on, the "Parabolic" BID shown in the first column refers to the union of this $A_1A_2B_1$ BID and its reflection $A_1B_1B_2$. In our TCGA analysis, this Parabolic BID frequently finds a Mixture data pattern. Similarly, the "W" BID in the second column refers to the union of this A_2B_1 BID and its reflection A_1B_2 . This W BID tends to find a particular Bimodal pattern in our TCGA data. The rows of Figure 4 are the four contexts. The top gene pairs are shown for each. The number of significant pairs for each BIDs is displayed at the top of each panel. No pair is shown for the Her2/LumB context with the BID $A_1A_2B_2$ because there is no significant pair of genes.

Figure 4 shows the Parabolic BID in the first column, which contains the largest number of significant pairs for each context. In those cases, some obviously show mixtures of different subtype distributions, such as the red Basal subtype in the lower right of the top row and the magenta Her2 cases in the lower right of the Her2/LumB context. The other relationships look strong but are not explained by subtypes, perhaps motivating additional genomic research. A more detailed discussion of the gene pair in the upper left appears in Section 3.3; of the gene pair in the lower left in Section 3.4.

Some surprising bimodal patterns in column 2 are captured by the W BID, which seem not to be driven by the breast cancer subtype information. In Section 3.5, we discuss the gene pair on the top row of column 2. To investigate the potential biological relevance of this bimodal dependence, an independent data set is used and discussed in Section 4.1.

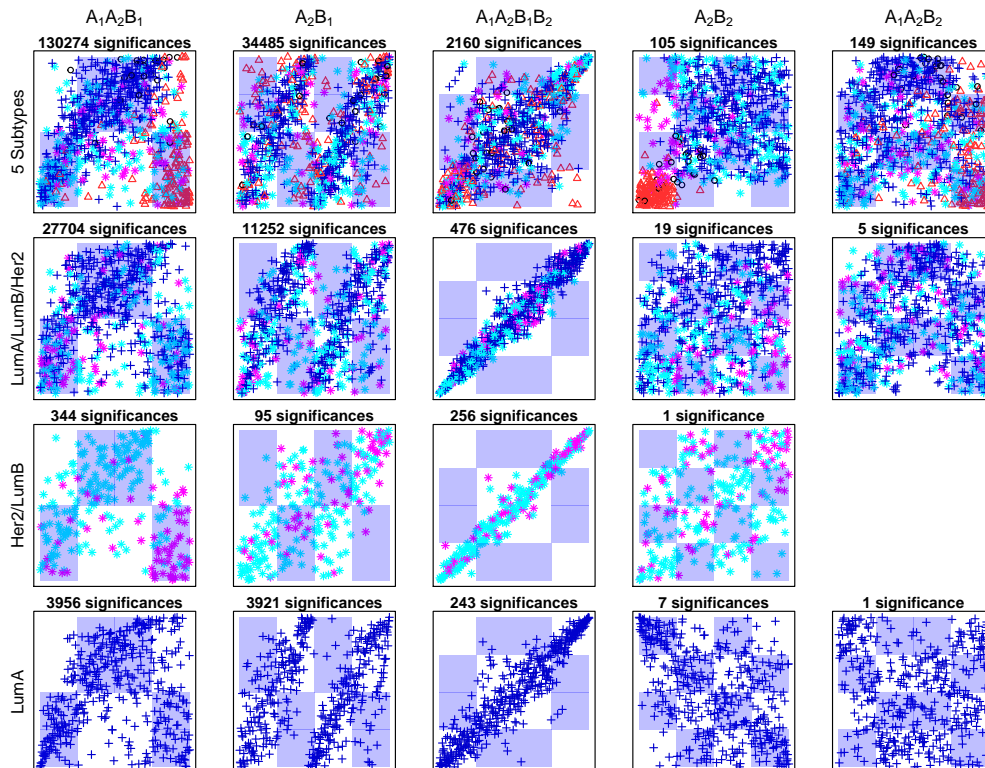


Figure 4: BET diagnostic plots where the four contexts are the rows and the five nonlinear BIDs are the columns. A most significant pair is shown for each. The number of significant pairs for each BIDs is shown at the top. There is no significant pair for Her2/LumB at $A_1A_2B_2$.

In column 3, some approximately linear pairs of genes are detected by the BID $A_1A_2B_1B_2$. In Section 3.6, we analyze the top pair in column 3 to discuss the connection between linearity and this nonlinear dependence pattern.

3.3 Mixture Pattern for Five Subtypes

In this section, we discuss the pair of genes shown in the top panel of Figure 5: ANKS6 and JAM3, which has the most significant mixture dependence pattern. The dependence of these two genes is captured by the blue region of this BID. From the log-scale scatter plot (top-right) and BET diagnosis plot (top-left) in Figure 5, it is visually apparent that the Basal subtype group is separated from the other subtypes. In particular, the non-Basal cases look like a classical bivariate Gaussian distribution and show a positive correlation between ANKS6 and JAM3 (larger values of ANKS6 lead to more expression of JAM3), while Basal behaves very differently: larger ANKS6 goes along with smaller JAM3. Here we revisit the reflection issue from the end of Section 2.2. ANKS6 in this example is the main driver of the separation between Basal and the others, and it will give the reflected pattern have the ordering of these two genes been reversed. Further insight comes from splitting the blue region into three rectangular regions (see the top-left panel) and calculating the respective proportions of the four breast cancer subtypes (ignoring the Normal-like) in each rectangle (bottom panels). These proportions reveal how the subtypes drive this relationship. Region 1 summarizes the lower left region of this unusual dependence; Region 2 summarizes the top part of this dependence; Region 3 summarizes the lower right region.

In the proportion bar plots, LumA and LumB subtypes have high proportions in Region 1 and

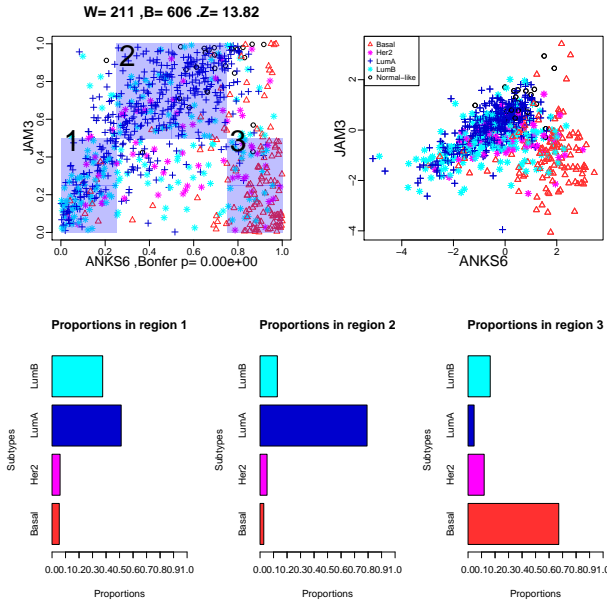


Figure 5: Top-left: BET diagnosis plot for the pair of genes: ANKS6 and JAM3, which shows a strong surprising dependency with large z-statistic value and three blue rectangular regions; Top-right: the scatter plot of the same two genes in the normalized log count scale after pre-processing. Bottom: the proportions for each breast cancer subtype (except normal-like) in each blue rectangular region.

Table 4: Observed counts for four breast cancer subtypes in three blue regions.

| Subtypes | region 1 | region 2 | region 3 |
|----------|----------|----------|----------|
| Basal | 9 | 8 | 90 |
| LumA | 86 | 229 | 6 |
| LumB | 63 | 37 | 22 |
| Her2 | 10 | 15 | 16 |

2. Those two subgroups account for 88.7% and 92% in the two regions separately, where the Basal subgroup only accounts for 5.4% and 2.8%. However, in Region 3, the proportion of Basal reaches 67%, and the total proportion of LumA and LumB is 21%. This observation indicates that the positive correlation of the LumA and LumB domains are in Regions 1 and 2, and the differing Basal correlation is in Region 3. The Pearson Chi-square test of independence is used to confirm this observation, for the counts of points in Table 4.

The p-value of this Chisq test is smaller than 2.2×10^{-16} (i.e., smaller than floating-point round-off error), and it shows a strong significance that these four subtypes are not homogeneously distributed in blue regions. To more directly validate the separation between Basal and the others, all others are combined into a single group and the Chi-square test gives another small p-value less than the round-off error. This result confirms the observation that this dependence pattern captured by the blue regions is very strongly significant and is influenced by the mixture of Basal and other subtype distributions.

The relationships between pairs of genes with respect to this same BID $A_1B_1B_2$ is shown by a network connection plot in Figure 6. Nodes in Figure 6 represent genes. This particular pattern of nonlinear BET dependence is highlighted by edges, which show Bonferroni statistical significance between genes. Furthermore, genes are ranked by their maximum BET z-scores. As shown in Figure 4, there are 130274 significant pairs of genes for this BID and its reflection. To avoid a too cluttered network graphic, only the top 200 genes are shown in Figure 6. These two hundred genes

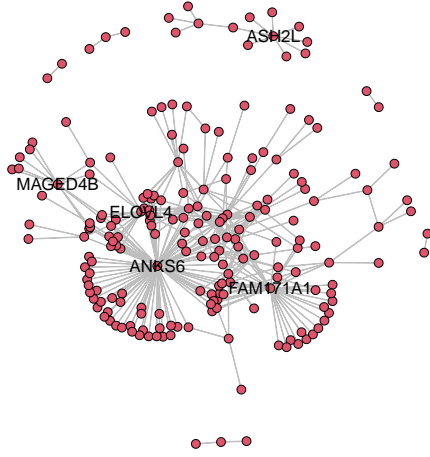


Figure 6: Connection plot of 200 most significant genes (nodes) with 311 edges for the BID $A_1B_1B_2$. Each node represents one gene and each edge represents a significant dependence between those genes. The large community illustrates there are many genes having significant mixture dependence pattern with the center gene, like ANKS6.

have 311 significant dependence edges for this Parabolic BID. Genes at the center of some visually important communities are labeled. Each community is a set of genes that shows this relationship with the center gene.

Good insights into a gene community and its functions come from finding where they appear among published gene signatures, such as those shown in The Molecular Signatures Database (MSigDB), a collection of annotated gene sets for use with Gene Set Enrichment Analysis [Subramanian et al., 2005, Liberzon et al., 2011, 2015]. We performed gene set enrichment analysis on each of the communities, and find that the gene set in the ANKS6 community is strongly associated with stromal or immune features. This is consistent with the previous finding that basal-like breast cancer has increased immune signature expression [Iglesia et al., 2016].

3.4 Mixture Pattern for Only Luminal A subtype

While subtypes have played an important role in the diagnosis and treatment of breast cancer, the heterogeneity of the disease motivates deeper investigation within subtypes. We focus only on the Luminal A breast cancer subtype observations. Figure 7 shows an additional interesting mixture dependence pattern in both the BET diagnosis (left panel) and log-scale scatter (right panel) plots. The right panel contains a positively correlated Gaussian point cloud on the left. There is a more diffuse cluster towards the lower right. This seems to indicate a mixture behavior. In particular, the gene ZDHHC2 bifurcates the data into a cluster where it is strongly positively correlated with CELF2, and another cluster where large values of ZDHHC2 correspond to small values of CELF2. Hence this pair of genes highlights potentially interesting subgroups, which could be the basis of further biological research.

The connection plot in Figure 8 shows which genes have many significant pairs within the 200 most significant genes in the LumA only context with the Parabolic BID. There are 190 significant dependence edges. This can be less than 200 because there are many pairs that only connect with each other. ZDHHC2 and FGF10 are two central genes having large communities, which motivate a

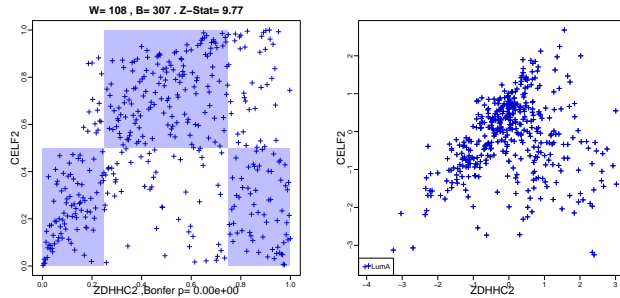


Figure 7: Left: BET diagnosis plot for a pair of genes which shows the mixture dependence within only the Luminal A subgroup; Right: The scatter plot of the same two genes in the normalized count scale. A point cloud with a strong positive correlation is on the left of the entire group and the remaining cases form a more diffuse cluster on the bottom-right. This could motivate deeper biological research into the LumA subtype.

deeper investigation. Checking carefully the individual plots reveals in all of these pairs, ZDHHC2 and FGF10 play the bifurcating role shown in Figure 7 in the dependence with each of these other genes.

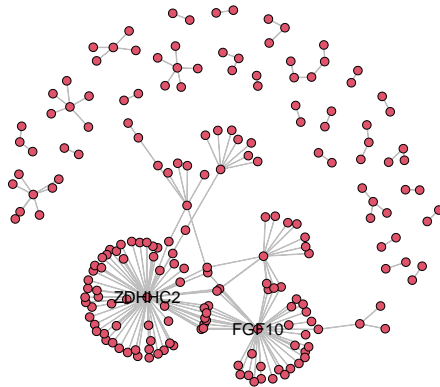


Figure 8: Connection plot of 200 most significant genes (nodes) with 190 edges for the Parabolic BID in the context of only Luminal A. ZDHHC2 and FGF10 are central genes in two large communities. The ZDHHC2 gene community has overlaps with some luminal gene sets in The Molecular Signatures Database (MSigDB).

To investigate the gene functions, we use gene set enrichment analysis again to compute overlaps between these communities and gene sets from MSigDB. This ZDHHC2 community has overlaps with some gene sets related to breast cancer, and in particular luminal subtype, such as CHARAFE_BREAST_CANCER_LUMINAL_VS_MESENCHYMAL_DN and CHARAFE_BREAST_CANCER_LUMINAL_VS_BASAL_DN [Charafe-Jauffret et al., 2006]. This confirms that ZDHHC2 and its community are an important player in luminal breast cancer and could motivate a deeper investigation into the role played by the ZDHHC2 community. On the other hand, a similar investigation of FGF10 doesn't show the connection with research to date on luminal breast cancer, again possibly motivating further biological work.

3.5 Bimodal Pattern

The second column of Figure 4 shows a perhaps surprising bimodal dependence pattern that is shared by many pairs of genes. The bimodal structure is strong in all contexts except Her2/LumB, suggesting that the Luminal A cases are a strong driver of this phenomenon. This may suggest

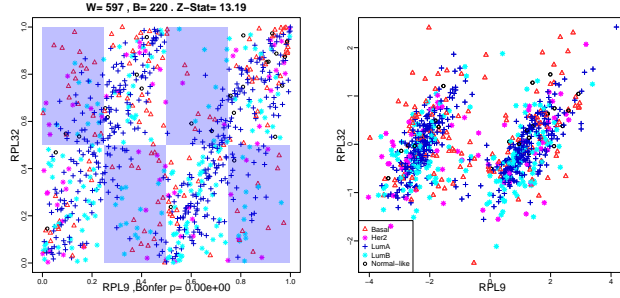


Figure 9: Left: BET diagnosis plot for a pair of genes that shows a bimodal dependence pattern; Right: The scatter plot of the same two genes in the normalized count scale. This bimodal relationship seems to be driven by Gene RPL9.

some fascinating biology.

To more deeply investigate this bimodal dependence, we take the top pair in the context of Five Subtypes as an example. Figure 9 shows the BET diagnosis (left panel) and log-scale scatter (right panel) plots of the most significant pair for this pattern in the context of Five Subtypes: RPL9 and RPL32. RPL9 in this pair separates the group into two positively correlated Gaussian clusters, suggesting this surprising bimodal dependence pattern perhaps is related to Gene RPL9.

To illustrate the correlation of this dependence with the Gene RPL9, in Figure 10 we use the connection figures of the top 200 genes (ranked by maximum BET z-score) for this pattern in the contexts of Five Subtypes (left panel), LumA (right panel) and of the only 174 significant genes in the Her2/LumB context (middle panel). The numbers of significant dependence edges for the Five Subtypes, Her2/LumB and LumA contexts are 152, 95 and 141.

From Figure 10, in the contexts of the Five Subtypes and LumA only which include LumA, RPL9 has large gene communities, in the sense of RPL9 showing this bimodal dependence with many genes. However, in the Her2/LumB context, there is no significant pair with RPL9 nor even a large community. Hence, this data set seems to suggest that the Gene RPL9 plays the main role in the significance pairs of this pattern, and perhaps is highly related to LumA. An important question is whether this finding is reproducible across data sets. In Section 4.1, we investigate this with an independent test set where this phenomenon is not observed, suggesting it is caused by some preprocessing steps particular to this data set.

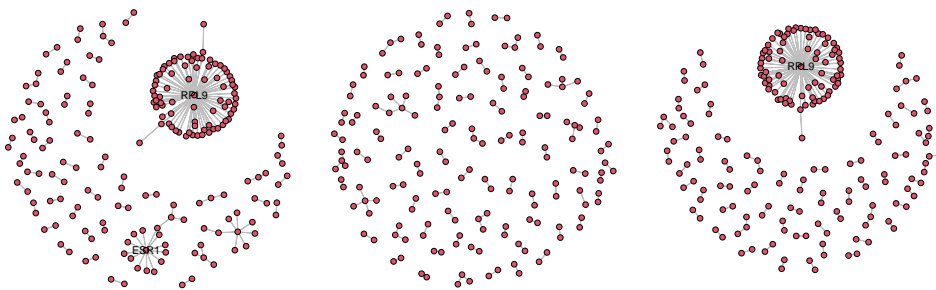


Figure 10: Left: Connection plot of the 200 most significant genes (nodes) with 152 edges in the context of Five Subtypes for the W BID; Middle: Connection plot of 174 significant genes with 95 edges in the context Her2/LumB for the same BID; Right: Connection plot of the 200 most significant genes with 141 edges in the context of LumA only for the same BID. RPL9 has a large community in each context including LumA for this bimodal dependence, but does not show such a pattern in the context with no LumA.

3.6 Connection between Linear and Nonlinear Patterns

In column three of the summary plot Figure 4, some approximately linear pairs of genes with a second-order structure are detected by the BID $A_1A_2B_1B_2$. In the middle panel of Figure 11, the top raw pair of genes in column 3: PROSC and ASH2L shows a linear relationship with strong skewness along the major axis. The left panel gives the BID diagnosis of this pair with the largest symmetry statistic value and z-score in all nine BIDs shown in Figure 4. To analyze the connection between this pair and the linear dependence BID A_1B_1 , we show the linear BID in the right panel. The corresponding counts of white and blue regions for BID $A_1A_2B_1B_2$ in the left panel are 607 and 210, so that the symmetry statistic S and the z-score are 397 and 13.89; the corresponding counts for the linear BID in the right panel are 599 and 218, so that the symmetry statistic S and the z-score are rather close, but slightly smaller values of 381 and 13.33. This suggests a different type of mixture model which may merit deeper investigation.

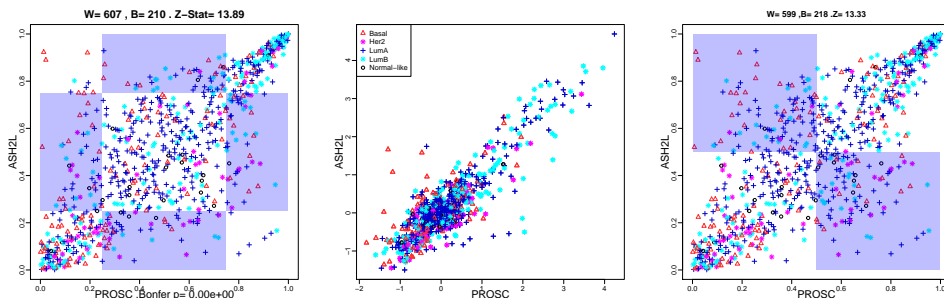


Figure 11: Left: The most significant BID diagnosis plot for a pair of genes: PROSC and ASH2L; Middle: The scatter plot of the same two genes in the normalized count scale; Right: The corresponding linear BID A_1B_1 for the same two genes. The value of each BET statistic for the linear BID is slightly smaller than that for the most significant BID.

4 Biological Reproducibility of TCGA Results

An essential issue with exploratory data analyses, as shown in Section 3 is their reproducibility. To investigate this for the interesting results shown in Sections 3.3 and 3.5, we consider an independent genomic data set: the Sweden Cancerome Analysis Network-Breast (SCAN-B) [Brueffer et al., 2018]. This data set came from the NCBI Gene Expression Omnibus (GSE96058). Data set was preprocessed as described in [Saal et al., 2015]. We use a subset of the gene expression data set which contains 2969 samples with full clinical data and 30865 genes. There are 15197 genes existing in both the SCAN-B and TCGA data sets. We only consider these common genes during this validation process. There was no further processing step in the SCAN-B set for our reproducibility analysis. First, in Section 4.1, we study the reproducibility of the Mixture patterns in the contexts of the Five Subtypes, as shown in Section 3.3. Then in Section 4.2, we find that the Bimodal pattern driven by Gene RPL9 in Section 3.5 is not observed in SCAN-B.

4.1 Biological Reproducibility of the Mixture Pattern

In Section 3.3, we find an interesting mixture pattern detected by the Parabolic BID in the context of the Five Subtypes. To investigate whether this mixture pattern is reproducible in the SCAN-B

data, we chose the most significant 200 genes for this context in TCGA results, as shown in the network connection plot Figure 6, along with the significant mixture pairs between them indicated as the edges. To understand the relationship between pairs over the two data sets, we rerun BET for these pairs in the SCAN-B data set and record the symmetry statistics and corresponding z-scores for the Parabolic BID instead of the most significant BID. Thus, we compare the significance for only the mixture pattern in these two data sets, as shown in Figure 12.

Within the top 200 genes for the Parabolic BID in TCGA, 7 out of these 200 genes do not exist in the SCAN-B, resulting in 298 significant (in TCGA) mixture pairs. To study the reproducibility of the mixture pattern of these pairs, we use a scatter plot to compare the z-scores of the Parabolic BID for TCGA on the vertical axis and the corresponding z-scores for SCAN-B on the horizontal axis, see Figure 12.

To show more clearly which pair in SCAN-B is as significant as in TCGA, we use the dark line $x = y$ to indicate the pairs whose z-scores in SCAN-B are more significant than those in TCGA. Because the sample size is much larger for SCAN-B, the black points to the right of that line tend to be higher in SCAN-B; hence the results tend to be more strongly significant. After visually checking, we find these pairs of genes show the same important mixture pattern of Basal and the other subtypes found in TCGA (see Figure 5). This illustrates the good reproducibility of this mixture pattern.

For the points to the left of that line, there tend to be two different types discussed using the colors shown in the plot. Typical behavior of the blue points is studied by showing the pair represented as a blue asterisk in Figure 12 in Figure 13. The BET diagnosis (left panel) and the SCAN-B scatter (middle panel) plots reveal a data threshold issue in the SCAN-B data set. The corresponding TCGA scatter plot (right panel) of this same pair in the right panel does not have this problem.

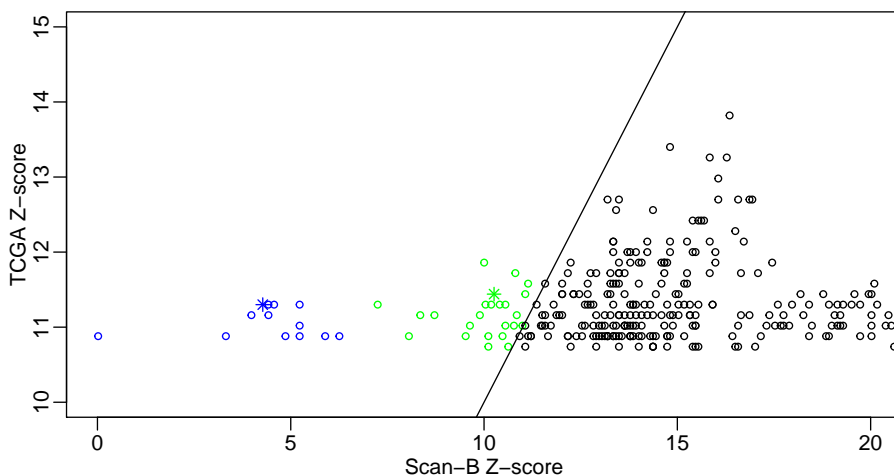


Figure 12: The scatter plot for the comparison of the Parabolic BID z-scores between the SCAN-B and TCGA data sets for the significant Mixture pairs within the top 200 genes in the Five Subtypes context of TCGA. The blue and green asterisk points are illustrated in Figures 13 and 14.

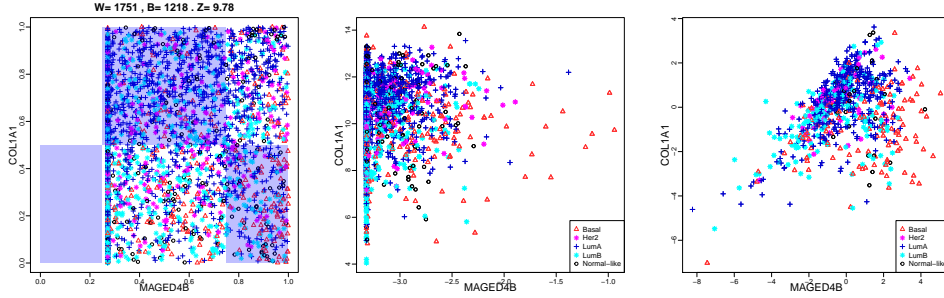


Figure 13: Left: BET diagnosis plot for a pair of genes in the SCAN-B that is shown as a blue asterisk in Figure 12 revealing a data threshold issue; Middle: The scatter plot of the same two genes in the original SCAN-B scale; Left: The scatter plot of the same two genes in the normalized TCGA count scale. This example represents a type of gene pairs which tend to be less significant in the SCAN-B data set.

Green pairs represent a different phenomenon as illustrated in Figure 14, which shows the pair highlighted with the green asterisk in Figure 12. The BET diagnosis (left panel) and the SCAN-B scatter (middle panel) plots definitely show the same behavior as in Figure 5, which is a clear separation between Basal and the other subtypes. However, the separation of the Basal is more distinct in TCGA, as shown in the TCGA scatter plot (right panel) of the same two genes, which is consistent with the more significant TCGA z-scores.

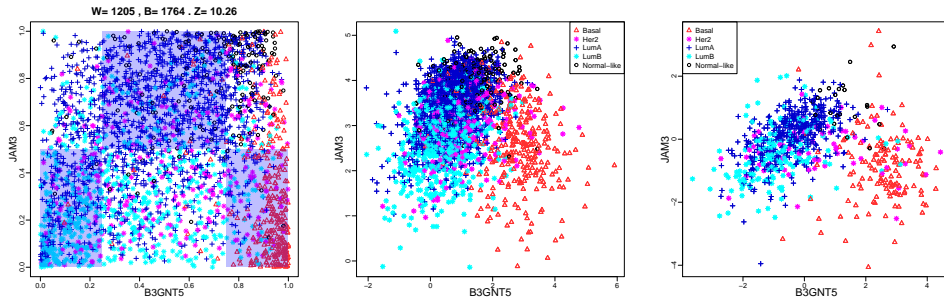


Figure 14: Left: BET diagnosis plot for a pair of genes in the SCAN-B data set that is shown as a green asterisk in Figure 12; Middle: The scatter plot of the same two genes in the original SCAN-B scale; Left: The scatter plot of the same two genes in the normalized TCGA count scale. This example represents gene pairs which tend to be less significant in the SCAN-B data set but still have the mixture pattern.

4.2 Lack of Reproducibility of the Bimodal Pattern

Here we study the pair of genes that gives the strongest Bimodal pattern signal in TCGA data set, which are RPL9 and RPL32 as shown in Figure 9. We rerun BET on this pair of genes in the SCAN-B data, and the strongest BID for this pair is linear, as shown in the left panel of Figure 15. Both the BET diagnosis (left panel) and the scatter (middle panel) plots show a relatively standard positively correlated linear dependence between RPL9 and RPL32. The right panel of Figure 15 gives the BET diagnosis plot for the W BID for this pair, which is much less significant than the linear pattern ($z = 30.85$ vs. $z = 10.96$). This shows that the surprising bimodal dependence observed in Figure 9 is not biologically reproducible. Instead, it seems to be a processing artifact that is not considered to be worth deeper investigation.

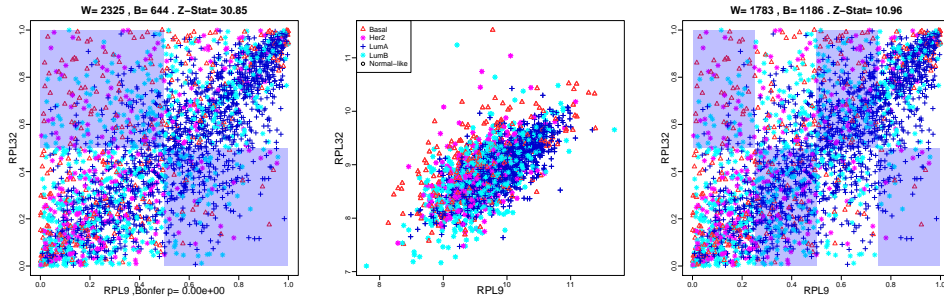


Figure 15: Left: BET diagnosis plot of the most significant BID (A_1B_1) for RPL9 and RPL32 in the SCAN-B data set; Middle: The scatter plot of the same two genes in the original SCAN-B scale; Right: BET diagnosis plot of the W BID for the same two genes. This shows the Bimodal pattern observed for RPL9 in TCGA data is not biologically reproducible.

Next, we test all genes with RPL9 in the SCAN-B data set and record the significant pairs whose strongest BID is the W BID. In the context of Five Subtypes, there are only 86 Bonferroni significant pairs among the 15196 pairs involving RPL9. We show the BET diagnosis (left panel) and the SCAN-B scatter (right panel) plots of the most significant pair in Figure 16. This pair shows a widely spread point cloud quite different from the bimodal pattern we observed above in TCGA data. That bimodal pattern is not reproducible in the SCAN-B W BID detection. A parallel analysis in the context of LumA only similarly shows no reproducibility of this particular Bimodal pattern.

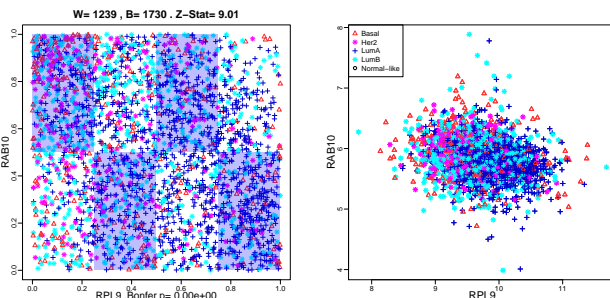


Figure 16: Left: BET diagnosis plot of the most significant pair of genes for the W BID in the SCAN-B data set; Right: The scatter plot of the same two genes in the original SCAN-B scale. The two distinct clusters present in Figure 9 are not present here, showing that is not reproducible.

5 Conclusion

TCGA gene expression data set is an important genomics data resource that shows many dependence patterns among genes, especially some interesting nonlinear dependence patterns. We use the computationally fast and powerful dependence testing method called BET to discover significant nonlinear dependence relationships in various contexts using the breast cancer subtypes information. We find that some interesting nonlinear dependence patterns are explained biologically by the mixture of the given breast cancer subtype distributions, such as the Mixture pattern for the context of Five Subtypes. Some relationships motivate further biological work, such as the Mixture pattern for the LumA only context. We also investigate the reproducibility of these results using an independent genomics data set. This shows that the mixture pattern is reproducible while the bimodal pattern related to the gene RPL9 is not and is apparently caused by some preprocessing

steps.

6 Acknowledgement

The results published here are in whole or part based upon data from the Cancer Genome Atlas managed by the NCI and NHGRI (dbGaP accession phs000178).

Xiang’s research was supported by SAMSI and NIH/NIAMS Grants P30AR072580 and R21AR074685.

Perou’s research was supported by NCI Breast SPORE program P50-CA58223 and U01CA238475-01.

Zhang’s research was partially supported by DMS-1613112, IIS-1633212, and DMS-1916237 from NSF.

Marron’s research was supported by NSF Grants IIS-1633074 and DMS-2113404.

References

- Christian Brueffer, Johan Vallon-Christersson, Dorthe Grabau†, Anna Ehinger, Jari Häkkinen, Cecilia Hegardt, Janne Malina, Yilun Chen, Pär-Ola Bendahl, Jonas Manjer, Martin Malmberg, Christer Larsson, Niklas Loman, Lisa Rydén, Åke Borg, and Lao H. Saal. Clinical value of rna sequencing–based classifiers for prediction of the five conventional breast cancer biomarkers: A report from the population-based multicenter sweden cancerome analysis network—breast initiative. *JCO Precision Oncology*, (2):1–18, 2018. doi: 10.1200/PO.17.00135. URL <https://doi.org/10.1200/PO.17.00135>. PMID: 32913985.
- E Charafe-Jauffret, C Ginestier, F Monville, P Finetti, José Adelaïde, N Cervera, S Fekairi, Luc Xerri, J Jacquemier, D Birnbaum, and F Bertucci. Gene expression profiling of breast cell lines identifies potential new basal markers. *Oncogene*, 25(15):2273–2284, April 2006. doi: 10.1038/sj.onc.1209254. URL <https://hal.archives-ouvertes.fr/hal-01431970>.
- Giovanni Ciriello, Michael L Gatz, Andrew H Beck, Matthew D Wilkerson, Suhm K Rhie, Alessandro Pastore, Hailei Zhang, Michael McLellan, Christina Yau, Cyriac Kandoth, et al. Comprehensive molecular portraits of invasive lobular breast cancer. *Cell*, 163(2):506–519, 2015.
- Wassily Hoeffding. A non-parametric test of independence. *Ann. Math. Statistics*, 19:546–557, 1948. ISSN 0003-4851. doi: 10.1214/aoms/1177730150. URL <https://doi.org/10.1214/aoms/1177730150>.
- Michael D. Iglesia, Joel S. Parker, Katherine A. Hoadley, Jonathan S. Serody, Charles M. Perou, and Benjamin G. Vincent. Genomic Analysis of Immune Cell Infiltrates Across 11 Tumor Types. *JNCI: Journal of the National Cancer Institute*, 108(11), 06 2016. ISSN 0027-8874. doi: 10.1093/jnci/djw144. URL <https://doi.org/10.1093/jnci/djw144>. djw144.
- Mark Kac. *Statistical independence in probability, analysis and number theory*. The Carus Mathe-

- mathematical Monographs, No. 12. Published by the Mathematical Association of America. Distributed by John Wiley and Sons, Inc., New York, 1959.
- Justin B. Kinney and Gurinder S. Atwal. Equitability, mutual information, and the maximal information coefficient. Proc. Natl. Acad. Sci. USA, 111(9):3354–3359, 2014. ISSN 0027-8424. doi: 10.1073/pnas.1309933111. URL <https://doi.org/10.1073/pnas.1309933111>.
- Alexander Kraskov, Harald Stögbauer, and Peter Grassberger. Estimating mutual information. Phys. Rev. E (3), 69(6):066138, 16, 2004. ISSN 1539-3755. doi: 10.1103/PhysRevE.69.066138. URL <https://doi.org/10.1103/PhysRevE.69.066138>.
- Arthur Liberzon, Aravind Subramanian, Reid Pinchback, Helga Thorvaldsdóttir, Pablo Tamayo, and Jill P. Mesirov. Molecular signatures database (MSigDB) 3.0. Bioinformatics, 27(12):1739–1740, 05 2011. ISSN 1367-4803. doi: 10.1093/bioinformatics/btr260. URL <https://doi.org/10.1093/bioinformatics/btr260>.
- Arthur Liberzon, Chet Birger, Helga Thorvaldsdóttir, Mahmoud Ghandi, Jill P. Mesirov, and Pablo Tamayo. The molecular signatures database hallmark gene set collection. Cell Systems, 1(6):417–425, 2015. ISSN 2405-4712. doi: <https://doi.org/10.1016/j.cels.2015.12.004>. URL <https://www.sciencedirect.com/science/article/pii/S2405471215002185>.
- Cancer Genome Atlas Network et al. Comprehensive molecular portraits of human breast tumours. Nature, 490(7418):61–70, 2012.
- Joel S Parker, Michael Mullins, Maggie CU Cheang, Samuel Leung, David Voduc, Tammi Vickery, Sherri Davies, Christiane Fauron, Xiaping He, Zhiyuan Hu, et al. Supervised risk predictor of breast cancer based on intrinsic subtypes. Journal of clinical oncology, 27(8):1160, 2009.
- Lao Saal, Johan Vallon-Christersson, Jari Häkkinen, Cecilia Hegardt, Dorthe Grabau, Christof Winter, Christian Brueffer, Man-Hung Eric Tang, Christel Reuterswärd, Ralph Schulz, Anna Karlsson, Anna Ehinger, Janne Malina, Jonas Manjer, Martin Malmberg, Christer Larsson, Lisa Ryden, Niklas Loman, and Ake Borg. The sweden cancerome analysis network - breast (scan-b) initiative: A large-scale multicenter infrastructure towards implementation of breast cancer genomic analyses in the clinical routine. genome med 2015. Genome medicine, 7:20, 02 2015. doi: 10.1186/s13073-015-0131-9.
- Aravind Subramanian, Pablo Tamayo, Vamsi K. Mootha, Sayan Mukherjee, Benjamin L. Ebert, Michael A. Gillette, Amanda Paulovich, Scott L. Pomeroy, Todd R. Golub, Eric S. Lander, and Jill P. Mesirov. Gene set enrichment analysis: A knowledge-based approach for interpreting genome-wide expression profiles. Proceedings of the National Academy of Sciences, 102(43):15545–15550, 2005. ISSN 0027-8424. doi: 10.1073/pnas.0506580102. URL <https://www.pnas.org/content/102/43/15545>.

- Ning Sun and Hongyu Zhao. Putting things in order. Proceedings of the National Academy of Sciences, 111(46):16236–16237, 2014. ISSN 0027-8424. doi: 10.1073/pnas.1418862111. URL <https://www.pnas.org/content/111/46/16236>.
- Gábor J. Székely and Maria L. Rizzo. Energy statistics: a class of statistics based on distances. J. Statist. Plann. Inference, 143(8):1249–1272, 2013. ISSN 0378-3758. doi: 10.1016/j.jspi.2013.03.018. URL <https://doi.org/10.1016/j.jspi.2013.03.018>.
- Gábor J. Székely, Maria L. Rizzo, and Nail K. Bakirov. Measuring and testing dependence by correlation of distances. Ann. Statist., 35(6):2769–2794, 2007. ISSN 0090-5364. doi: 10.1214/0090536070000000505. URL <https://doi.org/10.1214/0090536070000000505>.
- Leland Wilkinson, Anushka Anand, and Robert Grossman. Graph-theoretic scagnostics. In Information Visualization, IEEE Symposium on, pages 21–21. IEEE Computer Society, 2005.
- Kai Zhang. BET on independence. J. Amer. Statist. Assoc., 114(528):1620–1637, 2019. ISSN 0162-1459. doi: 10.1080/01621459.2018.1537921. URL <https://doi.org/10.1080/01621459.2018.1537921>.